Int J Adv Manuf Technol (2018) 95:875–888
https://doi.org/10.1007/s00170-017-1274-1

ORIGINAL ARTICLE

An optimal curvature-smooth transition algorithm with axis jerk limitations along linear segments

Yong Zhang[1,2] · **Peiqing Ye**[1,2] · **Jiaqi Wu**[1] · **Hui Zhang**[1,2]

Received: 6 June 2017 / Accepted: 26 October 2017 / Published online: 4 November 2017

Abstract Linear toolpath is generated by commercial computer-aided manufacturing (CAM) systems and it is most popular in computer numerical control (CNC) systems. Considering the discontinuity between two neighbor linear segments, corner feedrate is restricted and axis accelerations and jerks always exceed the given limitations, leading to low efficiency and poor accuracy, respectively. To overcome these two drawbacks, a novel curvature-smooth optimal transition algorithm and a jerk-continuous feedrate-scheduling scheme with axis jerk limitations are proposed in this paper. Firstly, based on the theoretical feedrate constraints with bounded axis accelerations and jerks, a quintic B-spline curve is adopted to generate curvature-smooth toolpath. To improve machining efficiency, corner feedrate is regarded as the optimal objective to determine the transition B-spline curve. Afterwards, considering the curvature-smooth toolpath, a corresponding five-phase jerk-continuous feedrate profile is provided to achieve higher machining precision. Finally, compared with curvature-continuous toolpath in simulations and experiments, the proposed algorithms can bound the axis kinematic parameters as expected and have advantages on improving machining precision especially under high kinematic limitations.

Keywords Quintic B-spline · Smooth curvature · Optimal transition algorithm · Axis jerk limitations · Jerk-continuous feedrate scheduling

✉ Hui Zhang
hui_zhang@outlook.com

[1] Department of Mechanical Engineering, Tsinghua University, Beijing 100084, China

[2] Beijing Key Laboratory of Precision/Ultra-precision Manufacturing Equipment and Control, Tsinghua University, Beijing 100084, China

1 Introduction

Parametric toolpath has been considered to be superior in machining efficiency and quality [1]. However, the shortcomings in accurate interpolation and suppression of feedrate fluctuation still exist [2, 3]. Thus, linear toolpath is still widely adopted in practical CNC systems [3] and it is significant to improve the performance for linear toolpath. Since corners of linear toolpath only have C^0 continuity, the velocity must be confined lowly. Consequently, frequently accelerating and decelerating contribute to the reduction in machining efficiency. Moreover, the acceleration and the jerk at corner points would also oscillate, resulting in serious vibration and poor surface texture. In order to deal with the problems, most researchers propose local corner transition and global curve-fitting methods to raise the toolpath smoothness and reduce contour error. Compared to curve-fitting methods [4–6], corner transition replaces corners with circular and parametric trajectory locally. Thus, it is high-efficient and transition error-constrained, making it widely implemented in CNC systems. Additionally, spline transition has the potential to fulfill continuous curvature and curvature derivative, which is significant to enhance geometric continuity. Thus, spline transitions, including Bezier and B-spline curves, are more popular than circle methods [7].

Du et al. [8, 9] utilized two symmetrical cubic Bezier curves and optimized the toolpath with curvature variation energy (CVE). Moreover, in order to obtain smoother toolpath, Fan et al. [10] applied two quartic Bezier curves to obtain G^3 continuous toolpath, and the advantages of G^3 continuity were elaborately compared with G^2 continuity. Subsequently, the transition algorithm was improved to obtain better characters [11] while the toolpath continuity is reduced to G^2. Sencer et al. [12] employed one quintic Bezier curve to blend the corners and gained G^2 continuity. The peak curvature was determined by offline numerical simulations and the

relations to corner angle were found and applied directly. Sun et al. [13] and Zhang et al. [14] presented a spline curve to obtain higher machining efficiency and better quality. However, the geometric continuity was not analyzed. To obtain smooth linear and circular segments, Pateloup et al. [15] proposed a non-uniform cubic B-spline while the curvature only can be calculated by simulation methods. Furthermore, Walton et al. [16] used quintic PH curves to blend sharp corners with theoretical curvature extreme; however, this method did not aim at CNC machining areas. Moreover, only tangential jerks, instead of axis jerks, are bounded in literatures [9–17], which cannot ensure machining quality especially in high kinematic limitations.

With the linear segments after smoothing, the next stage is to design a feedrate profile and schedule it along the transition toolpath. In this process, researchers have developed various methods including jerk-limited [18] and jerk-continuous acceleration/deceleration (ACC/DEC, AD) feedrate profiles. Zhao et al. [9] and Sun et al. [13] applied a polynomial jerk-limited feedrate-scheduling scheme in real-time CNC interpolator and a look-ahead method was also presented. In order to improve machining efficiency, Jahanpour et al. [19] proposed an S-shaped feedrate planning. Furthermore, Fan et al. [20] designed a time-optimal 15-phase AD profile with jerk-continuous feedrate and the superiority of the proposed profile was discussed over jerk-limited ones. In order to obtain a smoother AD profile, Lee et al. [21] and Wang et al. [22] proposed an offline feedrate-scheduling scheme and the continuous jerk was ensured by the trigonometric feedrate profile. Moreover, Huang et al. [23] utilized sine series to obtain optimal feedrate profile and the machining efficiency was slightly improved compared to Lee's method [21]. With the feedrate profile, Dong et al. [24] presented a generalized time-optimal bidirectional scanning algorithm with computational efficiency and robustness. Therefore, this scanning method is generally adopted in recent studies [9, 11].

In this paper, linear segments are improved to a G^3 continuous toolpath and the deduced corner feedrate constraints are utilized to optimize the corner feedrate to achieve better machining efficiency. Afterwards, feedrate scheduling with continuous jerk is provided. The reminder of this paper is organized as follows. A B-spline curve transition algorithm is presented to generate a G^3 continuous toolpath in section 2, and the middle control point is adjusted to obtain optimal corner feedrate considering axis jerks. Section 3 provides a novel jerk-continuous feedrate-scheduling scheme with axis jerk limitations, and a five-phase feedrate scanning is adopted. In section 4, the simulations and experiments are conducted to validate the proposed algorithms and the comparisons with previous methods are given in machining efficiency and contouring performance. Finally, the conclusions are given in section 5.

2 B-spline transition algorithms

2.1 B-spline curve

In order to generate a smooth toolpath, a quintic B-spline with nine control points is utilized between two adjacent linear segments. As shown in Fig. 1, its knot vector is [0 0 0 0 0 0 0.5 0.5 0.5 1 1 1 1 1 1]. The control points $\mathbf{P}_0$, $\mathbf{P}_1$, $\mathbf{P}_2$, $\mathbf{P}_3$ and $\mathbf{P}_5$, $\mathbf{P}_6$, $\mathbf{P}_7$, $\mathbf{P}_8$ lie on two linear segments, respectively, which means that the transition curve is tangential to two linear segments; hence, the toolpath is G^1 continuous at least. Considering the symmetry and local preserving property of B-spline curve, the control point $\mathbf{P}_4$, on the transition angular bisector, is adjustable to achieve better geometrical features. Based on de Boor-Cox algorithm, the quintic transition segment is defined parametrically as follows:

$$
\begin{aligned}
r(u) &= \sum_{i=0}^{8} A_i(u)\, P_i,\quad u \in [0,1] \qquad
A_4 = \begin{cases} 8u^4(5-8u), u\in[0,0.5] \\ 8(1-u)^4(8u-3), u\in[0.5,1] \end{cases} \\
A_0 &= \begin{cases} (1-2u)^5, u\in[0,0.5] \\ 0, u\in[0.5,1] \end{cases} \qquad
A_5 = \begin{cases} 8u^5, u\in[0,0.5] \\ 8(1-u)^3\left(31u^2-27u+6\right), u\in[0.5,1] \end{cases} \\
A_1 &= \begin{cases} 10u(1-2u)^4, u\in[0,0.5] \\ 0, u\in[0.5,1] \end{cases} \qquad
A_6 = \begin{cases} 0, u\in[0,0.5] \\ 40(1-u)^2(2u-1)^3, u\in[0.5,1] \end{cases} \\
A_2 &= \begin{cases} 40u^2(1-2u)^3, u\in[0,0.5] \\ 0, u\in[0.5,1] \end{cases} \qquad
A_7 = \begin{cases} 0, u\in[0,0.5] \\ 10(1-u)(2u-1)^4, u\in[0.5,1] \end{cases} \\
A_3 &= \begin{cases} 8u^3\left(31u^2-35u+10\right), u\in[0,0.5] \\ 8(1-u)^5, u\in[0.5,1] \end{cases} \qquad
A_8 = \begin{cases} 0, u\in[0,0.5] \\ (2u-1)^5, u\in[0.5,1] \end{cases}
\end{aligned}
\tag{1}
$$

In Fig.1, θ is half the angle between two adjacent linear segments and $\mathbf{e_x}$, $\mathbf{e_y}$, $\mathbf{e_z}$ are the unit orthogonal vectors along the spatial coordinate axes. For convenience, we assume $d_0 : d_1 : d_2 : d_3 : d_\Delta = 1 : k_0 : k_1 : k_2 : k_\Delta$ and denote $\lambda_i = d_0$

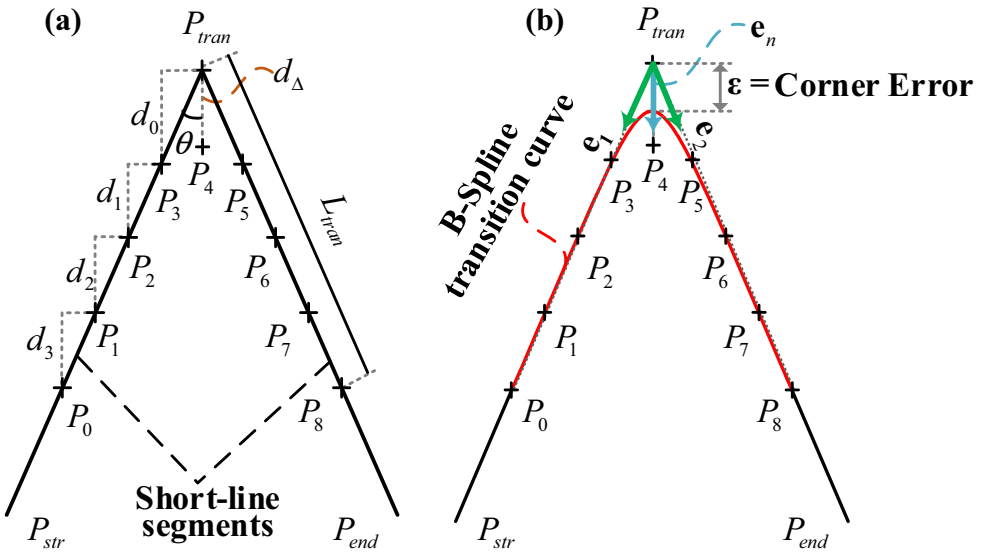

Fig. 1 Description of G^3 transition curve. **a** Control points. **b** B-spline transition curve

$\sec\theta\langle \mathbf{e_1}, \mathbf{e_i}\rangle$, $\mu_i = d_0\langle \mathbf{e_n}, \mathbf{e_i}\rangle$, $i = x, y, z$, where $\mathbf{e_1} = \mathbf{P_{tran}P_{str}}/\|\mathbf{P_{str}P_{tran}}\|$ and $\mathbf{e_n} = (\mathbf{e_1} + \mathbf{e_2})/\|\mathbf{e_1} + \mathbf{e_2}\|$ stand for the unit vector of linear segments and the transition angular bisector, respectively; hence, the control points yield:

$$\begin{aligned}
\mathbf{P_4} &= \mathbf{P_{trans}} + k_\Delta \sum_{i=x,y,z} \mu_i \mathbf{e_i} \\
\mathbf{P_3} &= \mathbf{P_{trans}} + \sum_{i=x,y,z} \lambda_i \mathbf{e_i} \\
\mathbf{P_2} &= \mathbf{P_{trans}} + (1 + k_0) \sum_{i=x,y,z} \lambda_i \mathbf{e_i} \\
\mathbf{P_1} &= \mathbf{P_{trans}} + (1 + k_0 + k_1) \sum_{i=x,y,z} \lambda_i \mathbf{e_i} \\
\mathbf{P_0} &= \mathbf{P_{trans}} + (1 + k_0 + k_1 + k_2) \sum_{i=x,y,z} \lambda_i \mathbf{e_i}
\end{aligned} \tag{2}$$

Thereafter, the toolpath continuity is discussed, and for convenience, the first and second derivatives of curve and curvature are denoted as:

$$\mathbf{r}_u = \frac{d\mathbf{r}}{du}, \mathbf{r}_{uu} = \frac{d^2\mathbf{r}}{du^2}, \kappa_u = \frac{d\kappa}{du}, \kappa_{uu} = \frac{d^2\kappa}{du^2} \tag{3}$$

Since there is only one double multiple-knot, $\mathbf{r}(u)$ has C^3 continuity at $u \in (0, 0.5) \cup (0.5, 1)$ and C^2 continuity at $\mathbf{P}_4$. In order to ensure C^2 continuity at junction points $\mathbf{P}_0$ and $\mathbf{P}_8$, normal vector must be zero, which can be achieved in the following equation:

$$\left.\begin{aligned} \mathbf{r}_{uu}|_{u=0} &= 0 \\ \mathbf{r}_{uu}|_{u=1} &= 0 \end{aligned}\right\} \Rightarrow k_2 = k_1 \tag{4}$$

For a 2D B-spline curves, $d\mathbf{r}/ds = \overrightarrow{T}$ and $d^2\mathbf{r}/ds^2 = \kappa\overrightarrow{N}$, where $\overrightarrow{T}, \overrightarrow{N}$ are the unit tangential and the normal vector and κ is the curvature; hence,

$$\frac{d^3\mathbf{r}}{ds^3} = \frac{d\kappa}{ds}\overrightarrow{N} + \kappa\frac{d\overrightarrow{N}}{ds} = \frac{d\kappa}{ds}\overrightarrow{N} - \kappa^2\overrightarrow{T} \tag{5}$$

In order to guarantee G^3 continuity, the continuity of curvature derivative is needed and it is expressed as follows:

$$\frac{d\kappa}{ds} = \frac{d\kappa}{du} \Big/ \frac{ds}{du} = \frac{\kappa_u}{|\mathbf{r_u}|} \tag{6}$$

Considering Eq. (1), $d\kappa/ds|_{u=0} = 0$ and $d\kappa/ds|_{u=1} = 0$ are qualified. When $u = 0.5$, the curvature derivative is calculated below:

$$\left.\begin{aligned} \left.\frac{d\kappa}{ds}\right|_{u=0.5^-} &= -\frac{96(k_\Delta - k_0 + 1)}{25d_0^2\tan^3\theta} \\ \left.\frac{d\kappa}{ds}\right|_{u=0.5^+} &= \frac{96(k_\Delta - k_0 + 2)}{25d_0^2\tan^3\theta} \end{aligned}\right\} \Rightarrow k_0 = k_\Delta + 1 \tag{7}$$

Obviously, $d\kappa/ds|_{u=0.5^-} = -d\kappa/ds|_{u=0.5^+}$, and considering G^3 continuous, $d\kappa/ds|_{u=0.5^-} = d\kappa/ds|_{u=0.5^+}$ is required; thus, $k_0 = k_\Delta + 1$ can be concluded.

All in all, the toolpath is G^3 continuous and the undetermined transition parameters are k_Δ, k_1.

2.2 Feedrate constraints

After transition, the linear segments are improved to the mixed trajectory of linear and spline segments, and the corner feedrate should be constrained to satisfy the acceleration and jerk limitations. In this case, the feedrate constraints are analyzed as follows.

The tangential velocity, acceleration, and jerk are denoted as v, a, j, respectively, and the arc length is assumed as s. Then, the vector forms of velocity, acceleration, and jerk are shown as follows [10]:

$$\begin{aligned} v &= v\frac{d\mathbf{r}}{ds} \\ a &= a\frac{d\mathbf{r}}{ds} + v^2\frac{d^2\mathbf{r}}{ds^2} \\ j &= j\frac{d\mathbf{r}}{ds} + 3av\frac{d^2\mathbf{r}}{ds^2} + v^3\frac{d^3\mathbf{r}}{ds^3} \end{aligned} \tag{8}$$

For the G^3 continuous toolpath, since the first, second, and third curve derivatives about arc length are continuous, continuous jerk can be obtained. In addition, according to Eq. (5), the kinematic parameters can be re-expressed as:

$$\begin{aligned} v &= v\overrightarrow{T} \\ a &= a\overrightarrow{T} + v^2\kappa\overrightarrow{N} \\ j &= \left(j - v^3\kappa^2\right)\overrightarrow{T} + \left(3av\kappa + v^3\frac{d\kappa}{ds}\right)\overrightarrow{N} \end{aligned} \tag{9}$$

To analyze the corner feedrate limitations, the feedrate at the corners is considered as a constant value, and the tangential acceleration and jerk at corners are equal to zero. Based on that, the kinematic parameters can be simplified:

$$\begin{aligned} v &= v_t\overrightarrow{T} + v_n\overrightarrow{N} = v\overrightarrow{T} \\ a &= a_t\overrightarrow{T} + a_n\overrightarrow{N} = v^2\kappa\overrightarrow{N} \\ j &= J_t\overrightarrow{T} + J_n\overrightarrow{N} = -v^3\kappa^2\overrightarrow{T} + v^3\frac{d\kappa}{ds}\overrightarrow{N} \end{aligned} \tag{10}$$

In Eq. (10), the coefficients on tangential and normal directions should obey acceleration and jerk limitations simultaneously. As a matter of fact, the limitations in these directions are usually equal to each other for CNC machines [1–3, 8–12]. Therefore, the tangential and normal kinematic limitations are set as $A_t = A_n = A_m$ and $J_t = J_n = J_m$ in this part, where A_m, J_m are the given maximum. Moreover, with the bounded tangential and normal kinematic parameters, the axis accelerations and jerks would also be limited [21]. Correspondingly, the feedrate constraints are given as follows:

$$\begin{aligned} v_{\lim}^A &= \sqrt{\frac{A_n}{\kappa}} \\ v_{\lim}^J &= \min\left(\sqrt[3]{\frac{J_t}{\kappa^2}}\sqrt[3]{,}\frac{J_n}{\kappa_s}\right) \end{aligned} \tag{11}$$

Furthermore, the tangential limitations of acceleration and jerk in Eq. (11) are consistent with conclusions in reference [17], which validates the process. In order to satisfy acceleration and jerk limitation simultaneously, the corner feedrate is determined by Eq. (12), where F is the command feedrate from G codes.

$$v = \min\left(v_{\lim}^A, v_{\lim}^J, F\right) \tag{12}$$

2.3 Determination of optimal transition curve

2.3.1 Scaling factor of transition curve

As shown in Fig. 1, considering the symmetry and convex hull property of B-spline curve, the maximum deviation from the original linear segments occurred at $u = 0.5$, and it is calculated as follows:

$$\varepsilon = \|\mathbf{P_4} - \mathbf{r}(0.5)\| = \frac{d_0}{2}(1 - k_\Delta) \tag{13}$$

The error constraint allowed by CNC systems is denoted as ε_m, then d_0 is constrained as $d_0 = 2\varepsilon_m/(1 - k_\Delta)$.

Assume the transition point is the coordinate origin, the corner error ε can be separated from the curve function, and the curve can be re-written as:

$$\mathbf{r} = \varepsilon\hat{\mathbf{r}} \tag{14}$$

Where $\hat{\mathbf{r}}$ is related to the transition parameters except corner error ε. Obviously, corner error ε can also be separated from $\mathbf{r}_u$ and $\mathbf{r}_{uu}$, which are utilized to calculate the curvature and its derivative. Besides, they are re-written as:

$$\begin{aligned} \kappa &= \frac{\|\mathbf{r_u} \times \mathbf{r_{uu}}\|}{\|\mathbf{r_u}\|^3} = \frac{\|\hat{\mathbf{r}}_\mathbf{u} \times \hat{\mathbf{r}}_\mathbf{uu}\|}{\varepsilon\|\hat{\mathbf{r}}_\mathbf{u}\|^3} = \frac{\hat{\kappa}}{\varepsilon} \\ \kappa_s &= \frac{d\kappa}{du}\Big/\frac{ds}{du} = \frac{\kappa_u}{\|\mathbf{r_u}\|} = \frac{\hat{\kappa}_u}{\varepsilon^2\|\hat{\mathbf{r}}_\mathbf{u}\|} = \frac{\hat{\kappa}_s}{\varepsilon^2} \end{aligned} \tag{15}$$

Therefore, corner error ε can simply scale the transition curve. Since the curvature and its derivative are independent of linear segments, the conclusion also applies to the situation that the transition point is not the coordinate origin. In other words, when the corner error increases, the transition curve will be zoomed in as a whole.

Considering Eqs. (11), (12), and (15), the corner feedrate limitations, which are restricted by acceleration and jerk, can be re-expressed as follows, where the coefficients $\alpha^A = \sqrt{\varepsilon A_m}, \alpha^J = \sqrt[3]{\varepsilon^2 J_m}$ are only determined by the given corner error ε and kinematic limitations A_m, J_m. Meanwhile, the coefficients have no relation with the smooth toolpath.

$$\begin{aligned} v_{\lim}^A &= \sqrt{\frac{A_m}{\kappa}} = \sqrt{\frac{\varepsilon A_m}{\hat{\kappa}}} = \frac{\alpha^A}{\sqrt{\hat{\kappa}}} \\ v_{\lim}^J &= \min\left(\sqrt[3]{\frac{J_m}{\kappa^2}}\sqrt[3]{,}\frac{J_m}{\kappa_s}\right) = \frac{\sqrt[3]{\varepsilon^2 J_m}}{\max\left(\sqrt[3]{\hat{\kappa}^2}\sqrt[3]{,}\hat{\kappa}_s\right)} \\ &= \frac{\alpha^J}{\max\left(\sqrt[3]{\hat{\kappa}^2}\sqrt[3]{,}\hat{\kappa}_s\right)} \end{aligned} \tag{16}$$

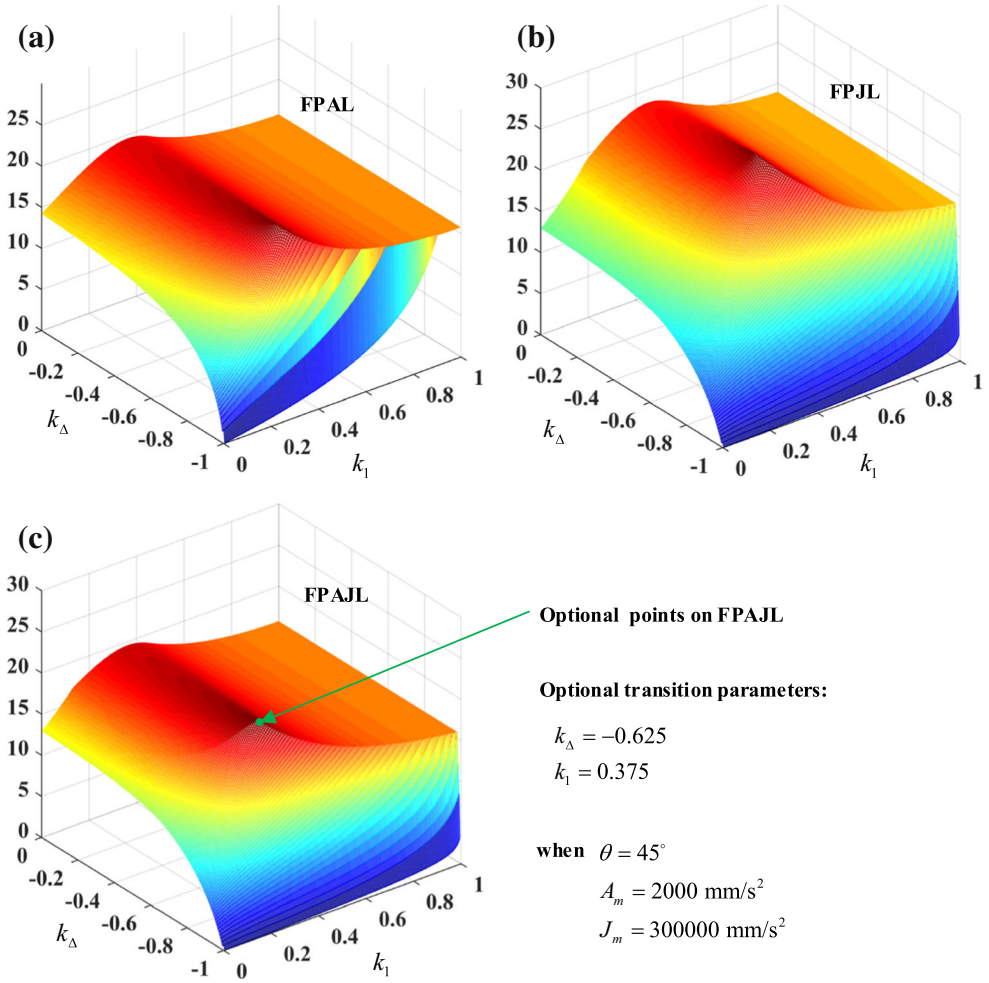

Fig. 2 Feedrate planes with acceleration and jerk limitations. **a** FPAL. **b** FPJA. **c** FPAJL

2.3.2 Transition optimization

For the B-spline transition curve, the global feedrate optimal parameters k_Δ, k_1 are searched to maximize the minimum value of the corner feedrate and the optimal objective is illustrated as follows:

$$v_{\lim} = \max_{k_\Delta, k_1} \left\{ \min \left[\min_u \left(v^A_{\lim} \right), \min_u \left(v^J_{\lim} \right) \right] \right\} \tag{17}$$

For a given corner error, the optimal method is conducted to any transition angle changed from 1° to 90° and the parameters k_Δ, k_1 are interpolated in the range of $[-1, 0]$ and $[0, 1]$. The curvature and its derivative are calculated at 500 discrete points along the transition B-spline parameter; thereafter, the curvature and its derivative extreme in Eq. (17) can be detected.

As shown in Fig. 2, for a given transition angle and kinematic limitations (45° and $A_m = 2000$ mm/s^2, $J_m = 300000$ mm/s^3 as examples), the corner feedrate with acceleration limitation (FPAL) and jerk limitation (FPJL) can be determined offline, respectively. In addition, corner feedrate with acceleration and jerk

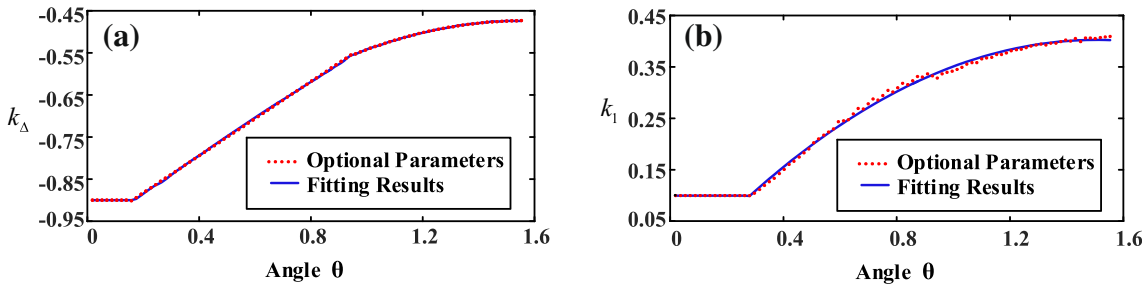

Fig. 3 The optimal parameters w.r.t transition angle. **a** k_Δ. **b** k_1

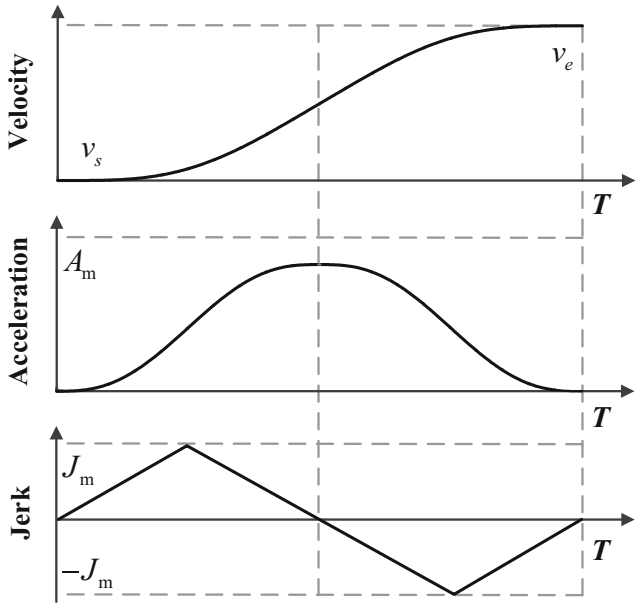

Fig. 4 An ACC period with jerk-continuous AD profiles

limitations (FPAJL) is combined by the smaller values of FPAL and FPJL, which is also shown in Fig. 2c. According to Eq. (17), the maximum of FPAJL is the optimal corner feedrate and the global feedrate optimal parameters k_Δ, k_1 are determined. Similarly, the optimal parameters can be searched for each transition angle from 1° to 90° as shown in Fig. 3.

In order to utilize the optimal transition curve in real-time CNC systems, a bisquare linear-fitting method is employed to obtain the relations between optimal parameters and transition angle, and the fitting results yield:

$$k_\Delta = \begin{cases} -0.9, 0 < \theta < 0.05\pi \\ -0.4407\theta - 0.9707, 0.05\pi < \theta < 0.3\pi \\ -0.2145\theta^2 + 0.6720\theta - 0.9997, 0.3\pi < \theta < 0.5\pi \end{cases}$$
$$k_1 = \begin{cases} 0.1, 0 < \theta < 0.089\pi \\ -0.2021\theta^2 + 0.6085\theta - 0.05474, 0.089\pi < \theta < 0.5\pi \end{cases} \quad (18)$$

Similarly, the curvature and its derivative, which are scaled by corner error from Eq. (15), can also be calculated offline to reduce the time cost on real-time motion plan process.

In the transition optimization process, the transition parameters k_Δ, k_1 are optimized under the given corner error and kinematic limitations. When these given parameters change, the optimal k_Δ, k_1 would vary correspondingly. In order to avoid the time-consuming process, FPAL, FPTJL, and FPAJL can be normalized and re-calculated by replacing the coefficients α^A, α^J with the new ones simply. Thus, a new FPAJL could be obtained efficiently and implemented in CNC systems directly.

3 Motion planning with G³ continuous toolpath

Based on Eq. (8), continuous jerk can be achieved for G^3 continuous toolpath, and compared to jerk-limited and trapezoid AD profile, jerk-continuous feedrate has advantages in

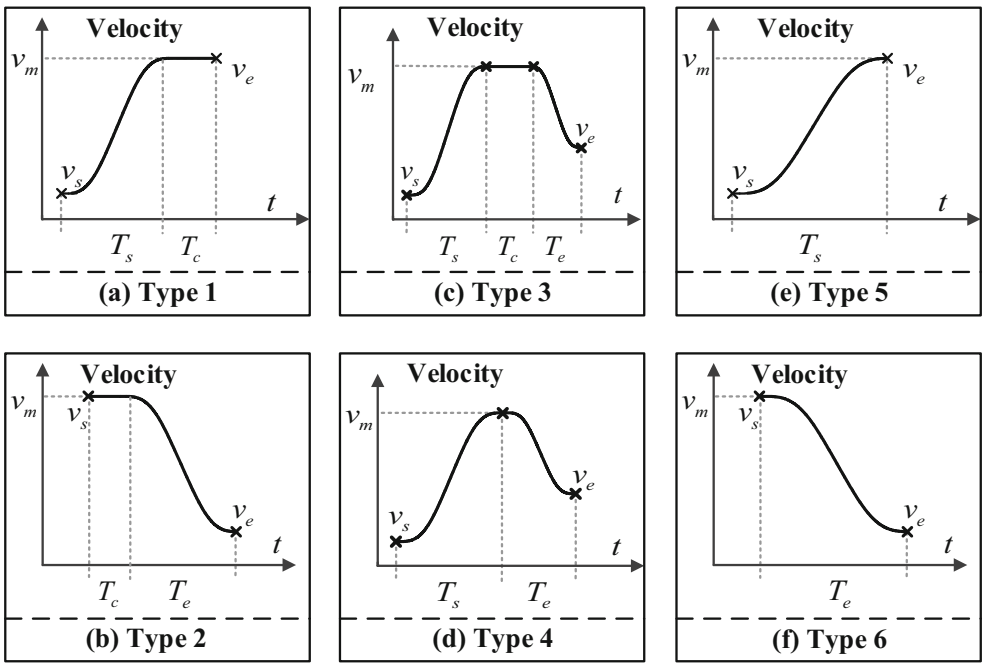

Fig. 5 All types of jerk-continuous AD profiles

Table 1 The AD parameters of all types

Type	Conditions	AD parameters
Type 1	$v_e = v_F$	$T_s = \sqrt{8(F-v_s)}\ /J_m, T_e = 0\ T_c = \left(L_i - \hat{L}_2\right)/F, v_m = v_F$
Type 2	$v_s = v_F$	$T_s = 0, T_e = \sqrt{8(F-v_e)}\ /J_m\ T_c = \left(L_i - \hat{L}_2\right)/F, v_m = v_F$
Type 3	$L_i < \hat{L}_2\ v_s \le v_e$	$T_s = \sqrt{8(v_e-v_s)}\ /J_m, T_e = 0\ T_c = 0, v_m = v_e$
Type 4	$L_i < \hat{L}_2\ v_s > v_e$	$T_s = 0, T_e = \sqrt{8(v_s-v_e)}\ /J_m\ T_c = 0, v_m = v_s$
Type 5	$L_i > \hat{L}_1$	$T_s = \sqrt{8(F-v_s)}\ /J_m\ T_e = \sqrt{8(F-v_e)}\ /J_m\ T_c = \left(L_i - \hat{L}_1\right)/F, v_m = v_s$
Type 6	$\hat{L}_2 < L_i < \hat{L}_1$	*Calculate* T_s by Eq.(29) $T_e = \sqrt{T_s^2 + 8(v_s-v_e)}\ /J_m\ T_c = 0, v_m = v_s + J_m T_s^2/8$

reducing vibration and improving the machining quality [25, 26]. In this section, a novel jerk-continuous AD profile is designed for the optimal G^3 continuous toolpath.

3.1 Jerk-continuous AD profile

A linear jerk profile is designed and the boundary conditions are shown in Eq. (19), where T is an ACC or DEC period.

$$\begin{cases} j(0) = j\left(\frac{T}{2}\right) = j(T) = 0 \\ j\left(\frac{T}{4}\right) = -j\left(\frac{3T}{4}\right) = J_m \end{cases} \tag{19}$$

Afterwards, the velocity, acceleration, and jerk can be obtained as follows:

$$j = \begin{cases} 4J_m \frac{t}{T} \\ -4J_m \frac{\left(t-\frac{1}{2}T\right)}{T} \\ 4J_m\left(\frac{t-T}{T}\right) \end{cases}, a = \begin{cases} 2J_m \frac{t^2}{T} \\ -J_m\left(\frac{2t^2}{T} - 2t + \frac{T}{4}\right) \\ J_m\left(\frac{2t^2}{T} - 4t + 2T\right) \end{cases}, \tag{20}$$

$$v = \begin{cases} v_0 + \frac{2}{3}J_m \frac{t^3}{T} \\ v_0 - J_m\left(\frac{2t^3}{3T} - t^2 + \frac{tT}{4} - \frac{T^2}{48}\right) \\ v_0 + J_m\left(\frac{2t^3}{3T} - 2t^2 + 2tT - \frac{13T^2}{24}\right) \end{cases}$$

The ACC profiles are shown in Fig. 4, where A_m and J_m are the tangential acceleration and jerk limitations, respectively.

From Eq. (20), the end velocity is expressed as follows:

$$v_T = v(T) = v_0 + \frac{1}{8}J_m T^2 \tag{21}$$

The period time is $T = \sqrt{8(v_T - v_0)/J_m}$ and the ACC or DEC block length yields:

$$L_i = s(\mathrm{T}) - s_0 = v_0 T + \frac{1}{16}J_m T^3 \tag{22}$$

Considering Eqs. (21) and (22), the jerk-determined feedrate v_T^J can be obtained by the following equation, and this equation can be solved by Newton-Raphson methods efficiently.

$$\left(v_T^J + v_0\right)^2\left(v_T^J - v_0\right) = \frac{1}{2}{L_i}^2 J_m \tag{23}$$

Moreover, the maximal acceleration occurs at the middle of ACC period and $a_m = a_{0.5T} = J_m T/4 < A_m$. Thus, the acceleration-determined feedrate v_T^A also needs to satisfy the following equation simultaneously.

$$v_T^A = \frac{2{A_m}^2}{J_m} + v_0 \tag{24}$$

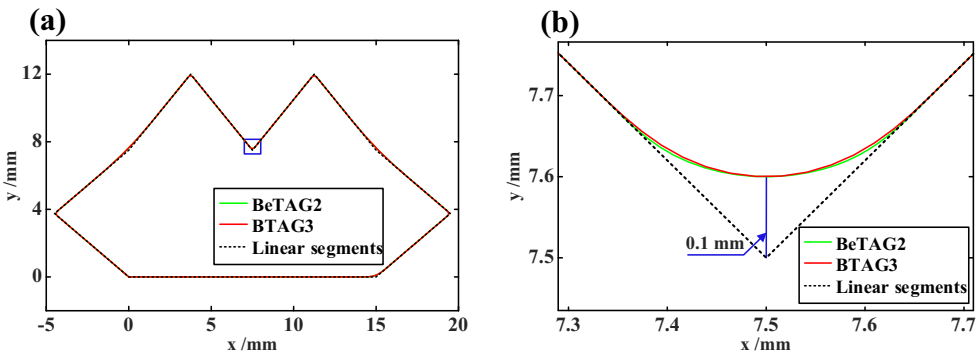

Fig. 6 Linear toolpath for BTAG3 and BeTAG2. **a** Toolpath smoothing. **b** Detailed transition results at sharp corners

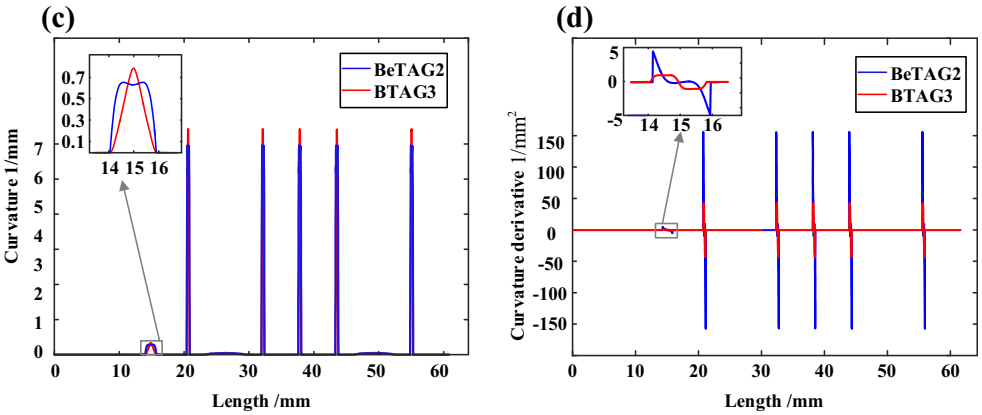

Fig. 7 The curvature and its derivative profile for BTAG3 and BeTAG2

3.2 Feedrate-scheduling scheme

In order to determine the reachable corner feedrate, a bidirectional scanning algorithm is implemented in feedrate scheduling and the procedure is generally illustrated in reference [9]. Different from reference [9], a jerk-continuous AD profile is adopted instead of the jerk-limited ones. In the stage of feedrate scheduling, the proposed AD profile is applied to connect the reachable corner feedrate and the procedure is similar to reference [21]. The main difference is that the toolpath is composed of linear and B-spline segments while that in reference [21] is a continuous NURBS curve.

In this part, the feedrate-scheduling parameters consist of feedrate and period ones. For feedrate parameters, we denote v_s, v_e, v_m as the start, end, and maximum velocities, respectively, while the period parameters are composed of the acceleration period T_s and the deceleration period T_e as well as the constant feedrate period T_c. Besides, the parameters to be determined are v_m, T_s, T_e, T_c.

All kinds of AD profiles are given in Fig. 5 and the type-determinant process is described in the following.

If the command feedrate occurred at the end position and $v_e = v_F$, it corresponds to type 1 in Fig. 5 while the condition $v_s = v_F$ means type 2. As shown in Fig. 5a, b, the CV (constant velocity) period exists in both cases. Otherwise, the AD profiles are illustrated as follows.

Firstly, if the AD block length is longer than the reference length L_{r1}, which means that the maximum feedrate is equal to the command one, thus ACC, CV, and DEC profiles exist. In this type, since $\max(v_e, v_s) < v_m = v_F$ and the determination of period parameters T_s, T_e, T_c is similar no matter $v_e > v_s$ or $v_e < v_s$, we give $v_e > v_s$ as an example and Fig. 5c provides the AD profile. Reference length L_{r1} is calculated as:

$$L_{r1} = (v_s + v_F)\sqrt{\frac{2(v_F - v_s)}{J}} + (v_e + v_F)\sqrt{\frac{2(v_F - v_e)}{J}} \quad (25)$$

Secondly, if the AD block length is shorter than the reference length L_{r2}, the length needed by accelerating or decelerating from v_s to v_e, only ACC or DEC profile exists. The AD profile is shown in Fig. 5e or f, and it corresponds to type 5 or 6. The reference length L_{r2} is calculated as:

$$L_{r2} = (v_s + v_e)\sqrt{\frac{2|v_s - v_e|}{J}} \quad (26)$$

Finally, if the block length L_i satisfies $L_{r2} < L_i < L_{r1}$, this case is type 4, and the maximum feedrate v_m is smaller than the command feedrate. The CV profile does not exist while ACC and DEC profiles exist. Similar to type 3, we also provide $v_e > v_s$ without loss of generality. In this type, with the acceleration period $T_s = \sqrt{15(v_m - v_s)}/2J_m$ and deceleration period $T_e = \sqrt{15(v_m - v_e)}/2J_m$, the relationship between T_s and T_e can be re-written as:

$$T_e = \sqrt{{T_s}^2 + \frac{8(v_s - v_e)}{J_m}} \quad (27)$$

Based on Eq. (22), the AD block length is also illustrated:

$$L_i = v_s T_s + \frac{1}{16} J_m {T_s}^3 + v_e T_e + \frac{1}{16} J_m {T_e}^3 \quad (28)$$

Considering Eq. (27), acceleration period T_s can be calculated by the following equation, where $\Delta v = v_s - v_e$.

Table 2 The comparisons between BTAG3 and BeTAG2

Algorithm	MC (1/mm)	CBE (1/mm)	MCD (1/mm^2)	CDBE (1/mm^3)
BTAG3	6.4	44.8	42.3	2234.7
BeTAG2	6.0	47.5	156.2	5945.2

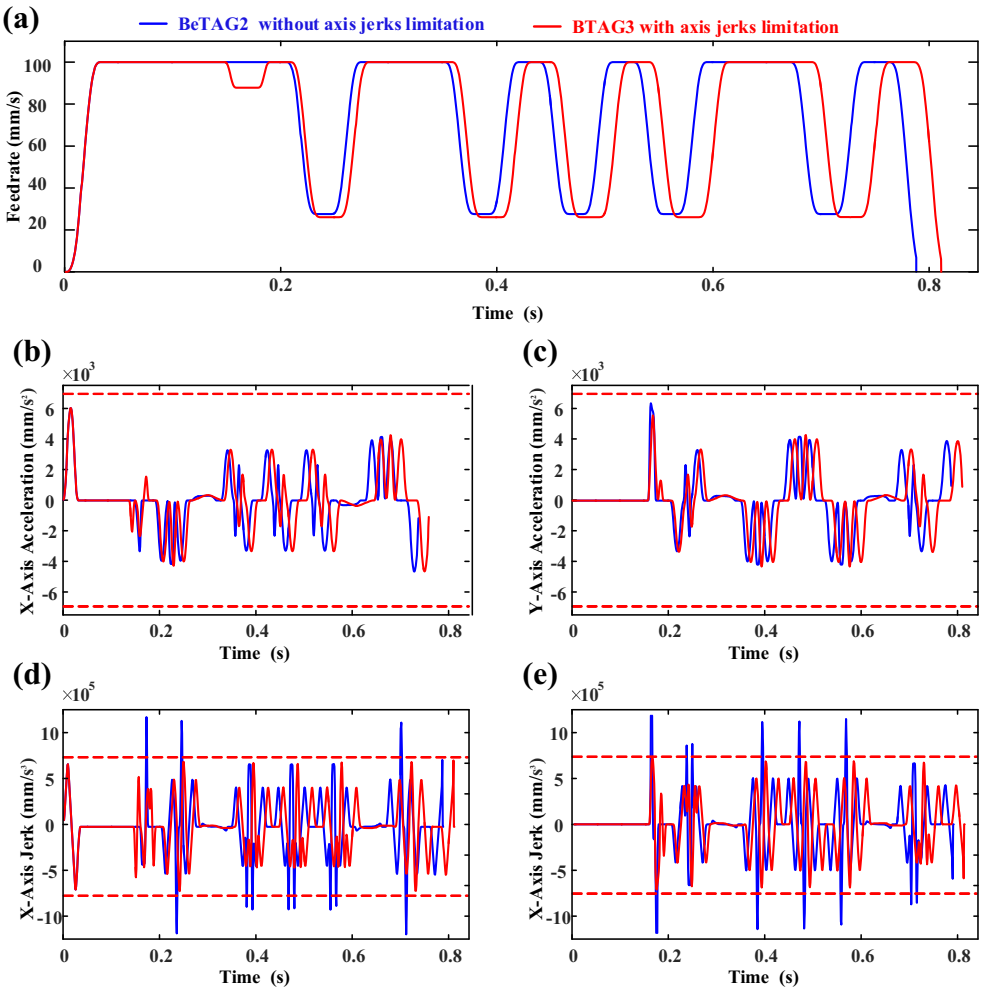

Fig. 8 The kinematic profiles for the linear toolpaths BTAG3 and BeTAG2. **a** Feedrate. **b** *X*-axis acceleration. **c** *Y*-axis acceleration. **d** *X*-axis jerk. **e** *Y*-axis jerk

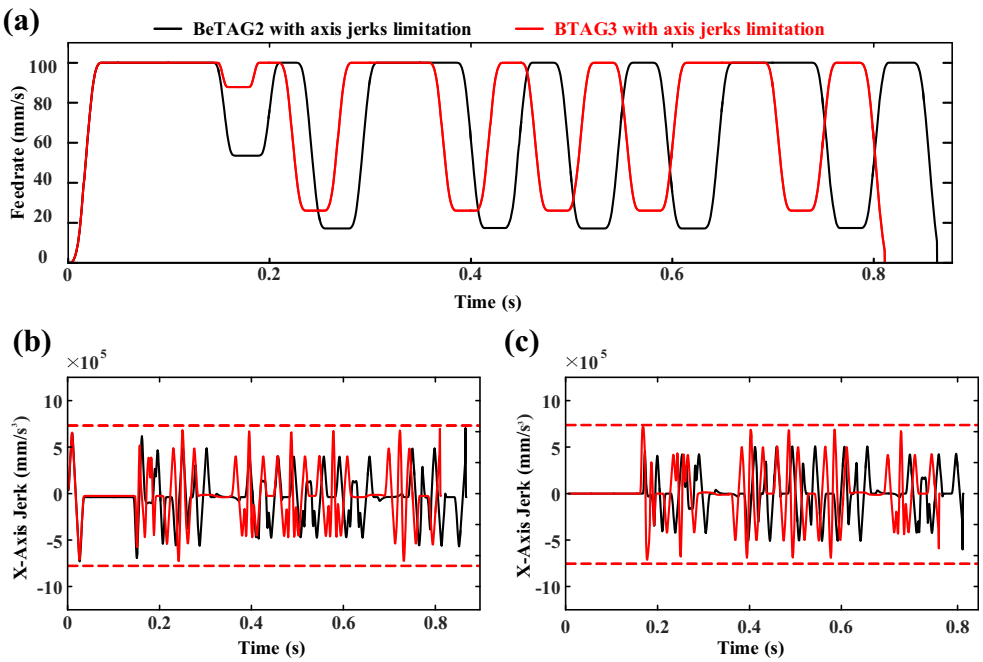

Fig. 9 The kinematic profiles for the linear toolpaths BTAG3 and BeTAG2. **b** *X*-axis jerk. **c** *Y*-axis jerk

Table 3 The comparison between BTAG3 and BeTAG2 with axis jerk limitations

Algorithm	BTAG3	BeTAG2
Cycling time	0.811	0.863
Cycle time reduction (%)	Base	6.4%

$$J_m \Delta v T_s{}^4 - 4 J_m L_i T_s{}^3 + 8 \Delta v^2 T_s{}^2 - 64 L_i v_s T_s + 32 L_i{}^2 - \frac{64}{J} \Delta v (v_e + v_s)^2 = 0 \tag{29}$$

In the end, parameters for all types of AD profiles are listed in Table 1.

After feedrate-scheduling process, the interpolation methods of linear and B-spline segments are generally applied in references [9, 20]. In order to reduce the feedrate fluctuation between linear segments and spline segments, a predictor-corrector interpolation method [27] is utilized in this step while the second-order Taylor interpolation is applied to other positions. Then, the sampling points can be computed in CNC systems and transferred to driver systems.

4 Simulations and experiments

In this section, the proposed algorithms are validated and compared with previous work in reference [12] where a G^2 continuous toolpath is obtained by quintic Bezier curve, and the minimal curvature is considered to determine the transition Bezier curve. For conciseness, the proposed B-spline transition algorithms with G^3 continuity and Bezier transition algorithms with G^2 continuity are abbreviated as "BTAG3" and "BeTAG2," respectively. For BTAG3, axis jerk limitations are considered while they are not bounded for BeTAG2.

4.1 Simulations

In this part, a linear toolpath is designed, and after path smoothing, the linear segments with G^0 continuity are enhanced to G^2 and G^3 continuous toolpaths, respectively, which are shown in Fig. 6a. The detailed path-smoothing results at sharp corners are zoomed in Fig. 6b. The corner error constraint is set as $\varepsilon = 0.1$ mm, and the jerk-continuous scheduling is done under kinematic constraints $v_m = 100$ mm/s, $A_m = 7000$ mm/s^2, and $J_m = 750000$ mm/s^3.

The curvature profile and curvature derivative profile are illustrated in Fig. 7a, b. And BTAG3 has smooth curvature and continuous curvature derivative, which guarantees more stable kinematic features for the vibration reduction. However, for BeTAG2, continuous curvature is obtained while its curvature derivative is uncontinuous as shown in Fig. 7b.

In order to evaluate the quality of toolpath, maximal curvature (MC) and curvature-bending energy (CBE) are defined in references [8, 10, 28]. Since axis jerks are bounded in this paper, maximal curvature derivative (MCD) and curvature derivative-bending energy (CDBE) are put forward for the first time. The CBE and CDBE have the following mathematical forms, where N is the number of corners. The results are shown in Table 2.

$$\begin{aligned} \mathrm{CBE} &= \int_0^s \|\kappa\|^2 ds = \sum_1^N \int_0^1 \|\kappa\|^2 |\mathbf{r_u}| du \\ CDBE &= \int_0^s \|\kappa_s\|^2 ds = \sum_1^N \int_0^1 \frac{\|\kappa_u\|^2}{|\mathbf{r_u}|} du \end{aligned} \tag{30}$$

Based on Table 2, BTAG3 has much lower CBE, MCD, and CDBE; hence, the toolpath generated by BTAG3 is

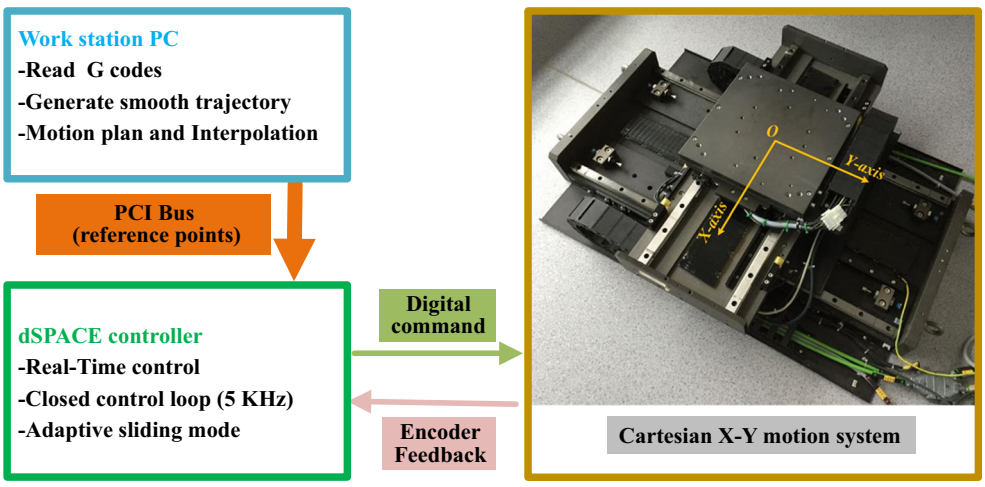

Fig. 10 Layout of the experimental platform

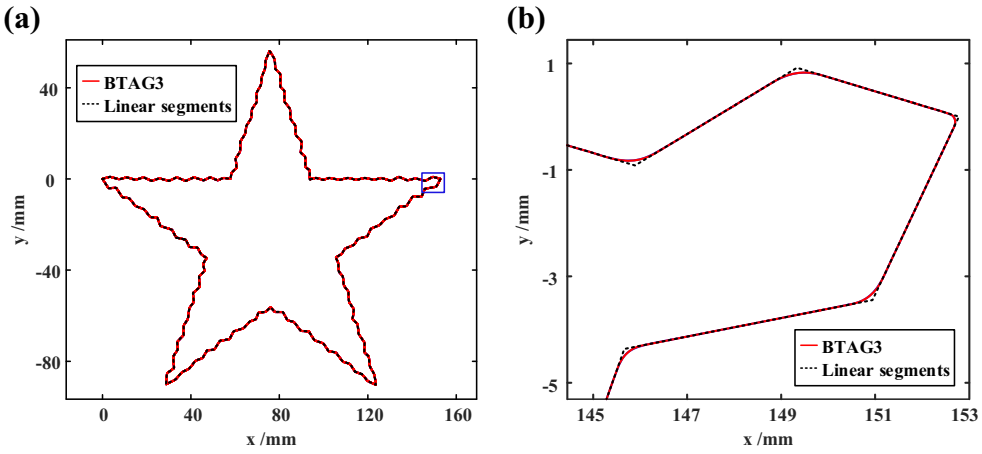

Fig. 11 Starfish toolpath for BTAG3. **a** Toolpath smoothing. **b** Detailed transition results at sharp corners

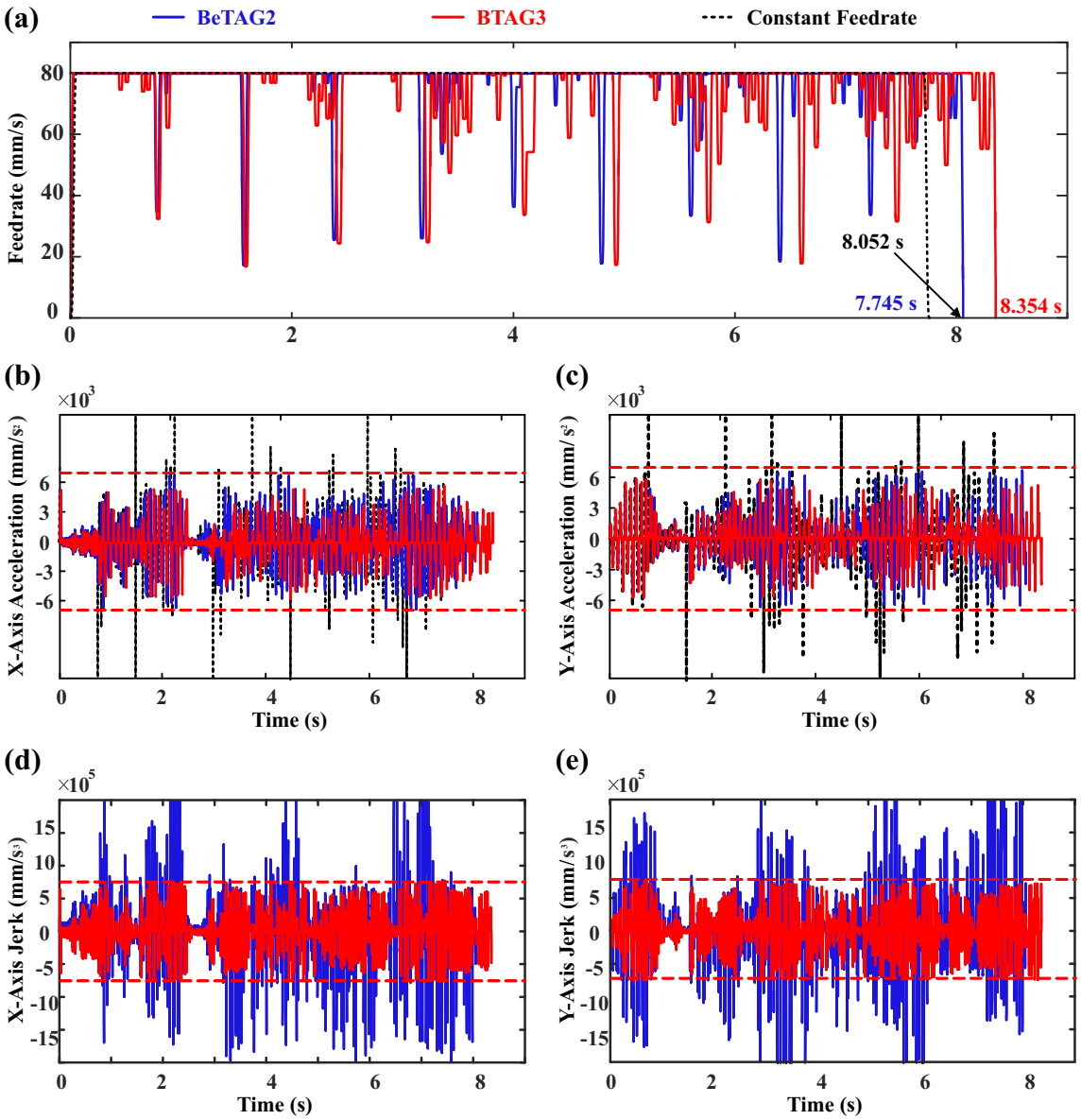

Fig. 12 The kinematic profiles for the starfish toolpaths BTAG3 and BeTAG2. **a** Feedrate. **b** *X*-axis acceleration. **c** *Y*-axis acceleration. **d** *X*-axis jerk. **e** *Y*-axis jerk

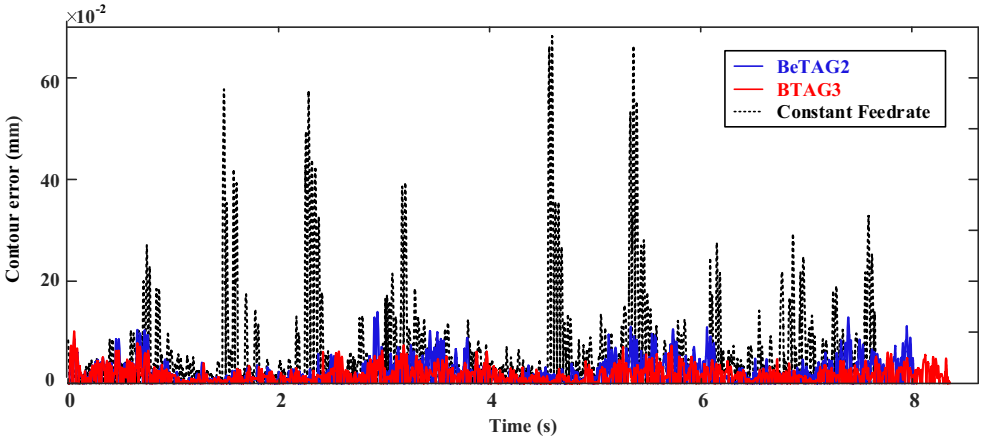

Fig. 13 Experimentally recorded contour error

smoother than BeTAG2. In the optimal process of BTAG3, maximal corner feedrate with axis jerk limitations, instead of minimal curvature, is taken as the optimal objective; thus, MC of BTAG3 is about 7% larger than that of BeTAG2. However, considering that the MCD of BTAG3 is about 70% smaller, the corner feedrate of BeTAG2 will become unavoidably slower when axis jerks are bounded.

Afterwards, for BTAG3 and BeTAG2, the simulation results are analyzed. The interpolation reference points are applied to compute the actual feedrate, axis accelerations, and axis jerks. As illustrated in Fig. 8, all of the actual values in terms of axis accelerations and axis jerks can be constrained within the setting limitations for BTAG3. When it comes to BeTAG2, the axis jerk limitations exceed greatly at sharp corners. However, for high-precision machining, the axis jerks should be bounded to reduce vibration and tracking error.

For BeTAG2, when axis jerk limitations are bounded with the same method in this paper, the feedrate and axis jerk profiles are elaborated in Fig. 9, and they are all subjected to the given limitations. However, the corner feedrate becomes much lower than that of BTAG3, and the machining efficiency is given in Table 3. Compared to BTAG3, the cycling time of BeTAG2 increases by about 6.4%.

4.2 Experiments

Experimental validations and comparisons between BTAG3 and BeTAG2 are performed on the Cartesian *X*-*Y* motion system driven by two linear motors. Current mode of servo amplifiers is set to validate the proposed algorithms. As shown in Fig. 10, a closed loop control is executed by a dSPACE 1202 real-time controller with an adaptive control model, and the closed loop sampling period is set as 0.2 ms. Linear encoders serve as position sensors with a resolution of 156.25 nm.

A more curvedly starfish curve is utilized to compare the performance between BTAG3 and BeTAG2 under jerk-continuous feedrate profile. The chord error constraint and the kinematic constraints are the same as that in simulations. Within the given tolerance, the G^3 continuous trajectory is shown in Fig. 11a, and the detailed path-smoothing results around several corners are shown in Fig. 12b.

The kinematic profiles of BTAG3 and BeTAG2 and the constant feedrate are shown in Fig. 12a. For the constant feedrate method, AD processes are not conducted around the sharp corners. Therefore, it has the shortest cycling time, which is 7.745 s; however, large violations of axis acceleration limitations exist in this strategy. Furthermore, since the axis jerks of constant feedrate motion are much larger than that of the other two methods, it is not given in Fig. 12d, e. BeTAG2 blend the corners by curvature-optimal Bezier curves and axis accelerations are bounded in feedrate scheduling. However, from Fig. 12d, e, axis jerk limitations are not respected. In contrast, the toolpath of BTAG3 is optimized to obtain the highest corner feedrate with axis jerk limitations; thus, the corner feedrate is reduced compared to other methods while the axis jerks are under limitations.

Table 4 Machining efficiency and contour performance

Methods	Cycling time (s)	Cycle time reduction (%)	Contour error (μm)		Mean contour error reduction (%)
			Max	Mean	
BTAG3	8.354	Base	100.624	17.453	Base
BeTAG2	8.052	− 3.62	141.181	23.875	36.80
Constant feedrate	7.745	− 7.29	683.253	65.694	276.41

Table 5 Machining efficiency and contour performance of different kinematic limitations

Kinematic limitations	Methods	Cycling time (s)	Cycle time reduction (%)	Contour error (μm)		Mean contour error reduction (%)
				Max	Mean	
$v_m = 60$ mm/s $A_m = 3500$ mm/s^2 $J_m = 300000$ mm/s^2	BTAG3	11.213	Base	90.165	10.936	Base
	BeTAG2	10.827	− 3.44	85.564	12.422	13.59
	Constant feedrate	10.340	− 7.79	520.185	28.024	256.25
$v_m = 70$ mm/s $A_m = 6500$ mm/s^2 $J_m = 500000$ mm/s^2	BTAG3	9.561	Base	89.552	13.240	Base
	BeTAG2	9.375	− 1.95	97.059	16.519	24.77
	Constant feedrate	8.862	− 7.31	607.777	39.597	199.07

The jerk profile would affect the contour errors and vibratory behavior of motors [26], and as shown in Fig. 13, the conclusion is verified in the tracking response. Since the closed loop bandwidths are limited, largest contouring errors occur at sharp corners. The machining efficiency and contour performance of the three methods are summarized in Table 4. Compared with BTAG3 proposed in this paper, the cycling time of BeTAG2 is reduced by about 3.62%; nevertheless, the maximal and mean contour errors increase a lot, and the mean contour error increases by nearly 36.80%. The constant feedrate motion has higher efficiency but the contour error is unacceptable.

For different kinematic limitations, the machining efficiency and contour performance of three methods have similar conclusions as shown in Table 5. With larger limitations, the contour performance of BTAG3 has more obvious improvement compared to BeTAG2 and the constant feedrate strategy.

5 Conclusions

A novel toolpath-smoothing algorithm with axis jerk limitations for linear segments is presented in this paper. The quintic B-spline transition curve is optimally designed to generate a curvature-smooth toolpath. Correspondingly, a five-phase jerk-continuous feedrate profile is designed and the feedrate scheduling with bidirectional scanning process is adopted. Compared to previous works, the proposed methodology has the following advantages: (1) the toolpath after transition satisfies G^3 continuous and can be scaled by corner error, which is rigorously constrained in path-smoothing algorithm; (2) the feedrate constraints with axis jerk limitations are given, and the smooth toolpath is optimized by maximizing the corner feedrate to improve machining efficiency; and (3) considering the trajectory continuity, continuous jerk is guaranteed in feedrate scheduling correspondingly. Finally, the proposed algorithms are validated by simulations and experiments compared to BeTAG2 and the constant feedrate strategy in efficiency and precision. The simulation and experiment benchmarks indicate that the proposed algorithms with bounded axis jerks can improve the contour performance dramatically with identical machining efficiency.

Acknowledgements The authors are grateful to Prof. Chuxiong Hu and Dr. Mingyong Zhao from Tsinghua University for the technical assistance in section 4.

Funding information This work was partially supported by the National Key Technology Support Program of China (No. 2015BAI0B16). The research was also supported by Guangdong ELESY Electric Co. Ltd.

References

1. Heng M, Erkorkmaz K (2010) Design of a NURBS interpolator with minimal feed fluctuation and continuous feed modulation capability. Int J Mach Tools Manuf 50:281–293
2. Zhang Q, Gao X, Li H, Zhao M (2017) Minimum time corner transition algorithm with confined feedrate and axial acceleration for nc machining along linear tool path. Int J Adv Manuf Technol 89:941–956
3. Zhang L, Sun R, Gao X, Li H (2011) High speed interpolation for micro-line trajectory and adaptive real-time look-ahead scheme in CNC machining. Sci China Technol Sci 54:1481–1495
4. Yang Z, Shen L, Yuan C, Gao X (2015) Curve fitting and optimal interpolation for CNC machining under confined error using quadratic B-splines. CAD Comput Aided Des 66:62–72
5. Ziatdinov R, Yoshida N, Kim T (2012) Fitting multispiral transition curve joining two straight lines. CAD Comput Aided Des 44:591–596
6. Wang Y, Yang D, Liu Y (2014) A real-time look-ahead interpolation algorithm based on Akima curve fitting. Int J Mach Tools Manuf 85:122–130
7. Pessoles X, Landon Y, Rubio W (2010) Kinematic modelling of a 3-axis NC machine tool in linear and circular interpolation. Int J Adv Manuf Technol 47:639–655
8. Du X, Huang J, Zhu L (2017) A locally optimal transition method with analytical calculation of transition length for computer numerical control machining of short line segments. Proc Inst Mech Eng Part B J Eng Manuf 95440541769735
9. Zhao H, Zhu L, Ding H (2013) A real-time look-ahead interpolation methodology with curvature-continuous B-spline transition scheme for CNC machining of short line segments. Int J Mach Tools Manuf 65:88–98

10. Fan W, Lee C, Chen J (2015) A realtime curvature-smooth interpolation scheme and motion planning for CNC machining of short line segments. Int J Mach Tools Manuf 96:27–46
11. Fan W, Lee C, Chen J (2016) Real-time repairable interpolation scheme for CNC tool path processing. Int J Precis Eng Manuf 17: 1673–1684
12. Sencer B, Ishizaki K, Shamoto E (2015) A curvature optimal sharp corner smoothing algorithm for high-speed feed motion generation of NC systems along linear tool paths. Int J Adv Manuf Technol 76: 1977–1992
13. Sun S, Lin H, Zheng L, Yu J, Hu Y (2015) A real-time and look-ahead interpolation methodology with dynamic B-spline transition scheme for CNC machining of short line segments. Int J Adv Manuf Technol 84:1359–1370
14. Zhang LB, You YP, He J, Yang XF (2011) The transition algorithm based on parametric spline curve for high-speed machining of continuous short line segments. Int J Adv Manuf Technol 52:245–254
15. Pateloup V, Duc E, Ray P (2010) Bspline approximation of circle arc and straight line for pocket machining. CAD. Comput Aided Des 42:817–827
16. Walton DJ, Meek DS (2009) G2 blends of linear segments with cubics and pythagorean-hodograph quintics. Int J Comput Math 86:1498–1511
17. Lai J, Lin K, Tseng S, Ueng W (2008) On the development of a parametric interpolator with confined chord error, feedrate, acceleration and jerk. Int J Adv Manuf Technol 37:104–121
18. Du D, Liu Y, Guo X, Yamazaki K, Fujishima M (2010) An accurate adaptive NURBS curve interpolator with real-time flexible acceleration/deceleration control. Robot Comput Integr Manuf 26: 273–281
19. Jahanpour J, Alizadeh MR (2015) A novel acc-jerk-limited NURBS interpolation enhanced with an optimized S-shaped quintic feedrate scheduling scheme. Int J Adv Manuf Technol 77:1889–1905
20. Fan W, Gao X, Yan W, Yuan C (2012) Interpolation of parametric CNC machining path under confined jounce. Int J Adv Manuf Technol 62:719–739
21. Lee A, Lin M, Pan Y, Lin W (2011) The feedrate scheduling of NURBS interpolator for CNC machine tools. CAD. Comput Aided Des 43:612–628
22. Wang Y, Yang D, Gai R, Wang S, Sun S (2015) Design of trigonometric velocity scheduling algorithm based on pre-interpolation and look-ahead interpolation. Int J Mach Tools Manuf 96:94–105
23. Huang J, Zhu LM (2016) Feedrate scheduling for interpolation of parametric tool path using the sine series representation of jerk profile. Proc Inst Mech Eng Part B J Eng Manuf 0954405416629588
24. Dong J, Stori JA (2006) A generalized time-optimal bidirectional scan algorithm for constrained feed-rate optimization1. J Dyn Syst Meas Control 2:384–390
25. Osornio-Rios RA, de Jesús R-TR, Herrera-Ruiz G, Castañeda-Miranda R (2009) FPGA implementation of higher degree polynomial acceleration profiles for peak jerk reduction in servomotors. Robot Comput Integr Manuf 25:379–392
26. Barre P, Bearee R, Borne P, Dumetz E (2005) Influence of a jerk controlled movement law on the vibratory behaviour of high-dynamics systems. J Intell Robot Syst Theory Appl 42:275–293
27. Yeh SS, Hsu PL (1999) The speed-controlled interpolator for machining parametric curves. CAD. Comput Aided Des 31:349–357
28. Xu G, Wang G, Chen W (2011) Geometric construction of energy-minimizing Bézier curves. Sci China Inf Sci 54:1395–1406